ELSEVIER

Computers & Geosciences 31 (2005) 371–384

COMPUTERS & GEOSCIENCES

www.elsevier.com/locate/cageo

A method to extract wave tank data using video imagery and its comparison to conventional data collection techniques ☆

Li H. Erikson*, Hans Hanson

Department of Water Resources Engineering, Lund University, Box 118, Lund 221 00, Sweden

Received 3 March 2003; received in revised form 24 September 2004; accepted 6 October 2004

Abstract

A procedure for obtaining quantitative wave and morphodynamic data in a laboratory setting using video images has been developed. The steps include image capture, rectification, and data extraction. All the necessary steps were maintained within the MATLAB environment so the process was streamlined and large amounts of data processed. The procedure involves the use of a program to rectify images, correcting for both lens distortion and camera position. A second program automatically extracts data from images to allow for high spatial and time frequency analysis. The method is shown to produce acceptable results as compared to more conventional methods of measuring wave and profile parameters in a wave tank experiment.

Keywords: Image analysis; Laboratory experiment; Automatic tracing; Wave shape; Profiles

1. Introduction

The use of video imagery to quantify hydro- and morphodynamic processes in a laboratory setting offers a number of advantages compared to conventional sampling systems. Of particular interest to coastal engineers and geomorphologists are the surf and swash zones where beach erosion or accretion occurs. The surf zone encompasses the region between the break point to some point near the shoreline, and the swash zone is that section of the foreshore that is alternately covered and exposed by wave uprush and backwash. When using gages to measure wave heights in the surf zone, large arrays are necessary to get good spatial coverage. The structure of the wave system between the gages is typically inferred from spectral analysis of current meters and wave gage records and synthetic spectra must be computed numerically to obtain a true picture of the wave structure (Sallenger and Holman, 1987). Video imagery, on the other hand, provides a spatial picture of the waveform and can be used on its own or to complement gage data and verify numerical calculations.

Measurement of swash hydrodynamics using conventional systems is often problematic due to low water depths, high velocities, and rapidly oscillating bi-directional currents (Foote and Horn, 1999a). Hughes (1992) found that conventional wave gages interfere with the flow in the swash zone and that it is most significant near the base of the beach where the maximum water velocities occur. He observed that disturbance of the water level could be as much as 2 cm or 10% of the swash depth. In movable bed experiments where swash gages are typically buried, pile-up of sediment behind the gage might occur and alter the flow dynamics.

☆Code on server at http://www.iamg.org/CGEditor/index.htm

*Corresponding author. Tel.: +1 831 476 8582.
E-mail address: li.erikson@sbcglobal.net (L.H. Erikson).

0098-3004/$ - see front matter © 2004 Elsevier Ltd. All rights reserved.
doi:10.1016/j.cageo.2004.10.006

Obtaining wave height measurements near dunes or beach scarps also poses problems when erosive events occur so that significant sand masses collapse and break gage wires located nearby. High-resolution morphological changes are cumbersome and sometimes difficult to measure, particularly if notching of a dune or scarp occurs. Video imagery offers a viable non-intrusive alternative to measure swash and morphodynamics in these regions.

The use of video equipment to record time-varying nearshore hydrodynamic and morphodynamic phenomena has been explored and refined over the past decades. The continued development of video camera technologies, particularly digital, provides opportunities for improvements to data collection techniques and data quality. Video imagery has been used for mostly qualitative but also for quantitative data collection in the field (e.g., Wright, 1976; Aagaard and Holm, 1989; Lippman and Holman, 1989, 1990, 1991; Holland et al., 1991; Holland and Holman, 1997; Redondo et al., 1994; Ruessink et al., 1998, 2002; Holland et al., 2001). The use of video cameras for quantitative data collection in the laboratory has also been explored but does not appear to be as well established (e.g., Smith and Kraus, 1990; Larson and Sunamura, 1993; Fenaish et al., 1989; Overton and Fisher, 1988; Overton et al., 1986; Foote and Horn, 1999a, b). As far as the authors are aware, no attempt has been made to use the advantages of a video camera as a single instrument to quantitatively measure both hydrodynamic and morphodynamic phenomena simultaneously in the laboratory. In addition, although video imagery has been used in the laboratory for quantitative measurement, little work has been done to validate the data. This study addresses these issues by comparing extracted data from video images to more conventional methods of measuring wave properties and profile changes. Foote and Horn (1999a) presented a method based on GIS software; the results were promising although the wave heights were often over-predicted. An alternative method, employing programs developed in the MATLAB environment, are presented in this paper.

In the following section, the basics behind videometrics and image distortion are reviewed. Sections 3 and 4 describe the laboratory set-up used for the experiment and post-processing techniques developed for this study. Measurements obtained from conventional instruments and video images are then compared.

2. Videometrics and image rectification

2.1. Videometrics

Videometrics can loosely be defined as the use of imaging technology to perform precise and reliable measurements of the environment. To understand the benefits, limitations, and need for post-processing of video images, a brief description of video cameras and the recording process is presented.

Video cameras contain several subsystems, of which the three most important are the lens, sensor, and recording mechanism. The lens provides a medium through which light is transmitted to the camera sensor, which measures the degree of optical wavelength electromagnetic energy. The recording mechanism calibrates and records the final signal. The precise design and manufacture of these systems determines the spatial, temporal, and radiometric quality of the resulting data.

Lens distortion is an optical error in the lens that causes differences in magnification of the object at different points on the image; straight lines in the real world may appear curved on the image plane. Since each lens element is radially symmetric, and the elements are typically placed with high precision on the same optical axis, this distortion is almost always radially symmetric and is referred to as radial lens distortion (Ojanen, 1999). Fig. 1 illustrates two types of distortion. The term barrel distortion is used to describe images that bulge toward the center, and pincushion distortion describes

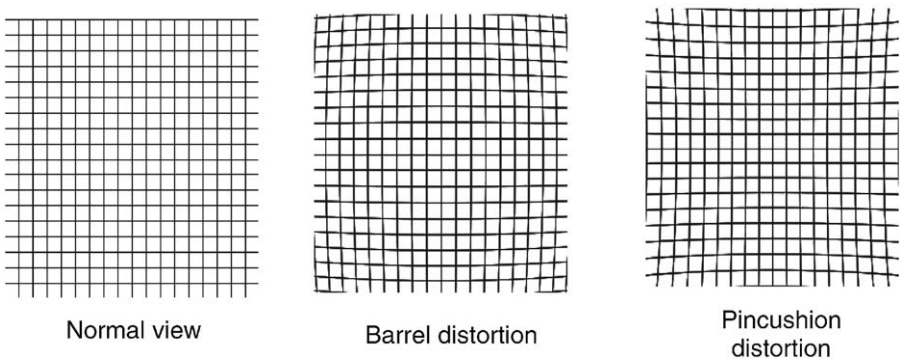

Fig. 1. Schematic sketch of barrel and pincushion distortion caused by camera lenses.

images shrinking toward the center. Most lenses exhibit both properties at different scales. Lens distortion has been shown to be the largest source of distortion error (compared to other types of intrinsic camera aberrations) and is typically the only type of distortion accounted for in computer video image processing (Tsai, 1987).

Signals captured from the physical world are translated into digital form by camera digitization. Camera digitizing involves both sampling and quantification. The image sensor or sampling device employed by most digital cameras and by the cameras used in this study is a charge-coupled device (CCD). The CCD is a silicon chip consisting of a two-dimensional array of photosites measuring the amount of light (photons) hitting it. A common analogy is an array of buckets. The photons can be represented as raindrops. As the raindrops fall in the bucket, water accumulates (i.e., electrical charge accumulates). Some buckets have more water and some buckets have less water, representing brighter and darker sections of the image. Keeping the analogy, an analog-to-digital converter measures the depth of the water and converts it to binary digital form. The recording mechanism typically works in one of two ways; either by reading the buckets row by row in ascending order or by reading all rows simultaneously. Progressive scanning is the term used to describe the former. Progressive scanning can be problematic with fast moving objects such as waves. In such a case, the top row would show the top of the wave at some fraction of a second before the bottom of the wave. The cameras employed for this experiment use CCDs that are *not* progressive scan and therefore the image of a wave is vertically synchronized in time within each half frame. The synchronization occurs only over half a frame because each still image from the video consists of two interlaced image fields taken consecutively: one field consists of odd numbered rows and the second field consists of even numbered rows. This is typical for off-the-shelf cameras at this time and is due to the standards set at the early days of broadcast television (Chapman and Chapman, 2000). Video cameras employing the phase alternating line (PAL) system sample at 1/25th of a second and contain two interlaced fields sampled at a time interval of 1/50th of a second. Since fields are actually separated in time, a fast moving object will change position between the fields and the edges will have a comb-like appearance as illustrated in Fig. 2. To prevent this effect one can de-interlace the image by either (1) averaging the two fields to construct a single frame, or (2) discard one of the fields (i.e., either the odd or even rows) and interpolate to obtain the missing information and obtain full frames. The latter method results in images with only half the vertical resolution (but full horizontal resolution) and with a doubled sampling frequency.

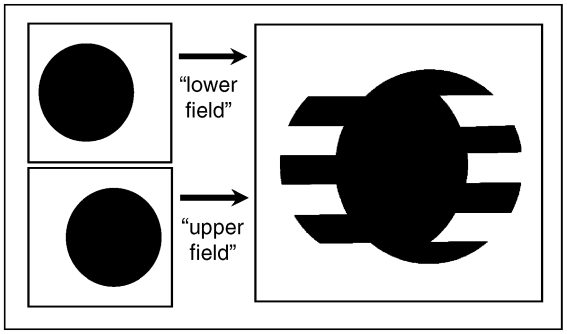

Fig. 2. Artifacts of fast moving objects filmed with camcorders employing interlaced fields.

2.2. Image rectification

Most image rectification procedures involve a two-step process (Ojanen, 1999; Holland and Holman, 1997): (1) calibration of intrinsic camera parameters, and (2) correction for a camera's extrinsic parameters (i.e., the location and rotation in space). The intrinsic parameters commonly required are the effective focal length, radial lens distortion coefficient, center coordinates of radial distortion on the camera's sensor plane (i.e., two parameters), and a scale factor to account for any aberrations caused when transferring data from the camcorder to the computer (Tsai, 1987). The extrinsic parameters consist of six variables describing the rotation and translation between real world and image coordinates. Thus, a total of 11 parameters (five intrinsic and six extrinsic) are required to translate three-dimensional space to a two-dimensional image plane.

Most existing methods for image rectification can be categorized as either implicit or explicit (Holland and Holman, 1997). An implicit scheme was employed for the study described in this paper. For this type of approach, coefficients that represent combinations of intrinsic and extrinsic parameters are determined from a set of linear equations that relate the actual position of an object to the position recorded on the image plane. Accuracy is governed by the number of control points employed. Non-linear effects can be accounted for with a large number of accurately positioned control points, but distortion between control points is always assumed to be linear.

Explicit methods are routinely applied by photogrammatists and involve determining all the camera parameters in terms of dimensional physical units (mm, radians, etc.). Precise knowledge of camera placement and tilt are required and the remaining parameters are typically estimated with an iterative algorithm that minimizes a set of non-linear or linearized equations. These sophisticated calibration models have the ability to obtain a high degree of accuracy from complicated forms of lens distortion and other systematic errors.

However, the use of non-linear equations can be cumbersome and initial approximations of unknown parameters can lead to diverging solutions.

Implicit methods may not provide the same degree of accuracy but are often quicker and less cumbersome to apply. Implicit schemes of image rectification are well suited for laboratory tank tests because they are rather quick, easy to apply, and do not require *a priori* knowledge of intrinsic camera parameters and precise measurement of camera position and tilt. Whether or not the implicit scheme provides sufficient accuracy is the purpose of this study. With a camera set-up as shown in Figs. 3 and 4, the aim is to transform points from a real world surface to a non-coplanar image plane. A rather simple method to perform this transformation, accounting for both intrinsic and extrinsic parameters simultaneously, was developed for this study.

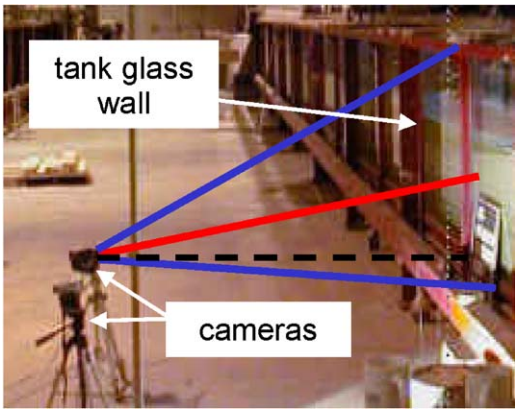

Fig. 3. Typical camera setup showing axis between camera lens and real world image plane.

3. Laboratory set-up and procedure

The experiment was conducted in a 27-m long wave tank at the US Army Engineer Research and Development Center, Coastal and Hydraulics Laboratory, in Vicksburg, Mississippi. The tank measured 0.91 m at maximum depth. The experimental set-up is shown in Fig. 4.

Dunes and fronting beaches were formed of uniform sand with a median grain size diameter (D_{50}) of

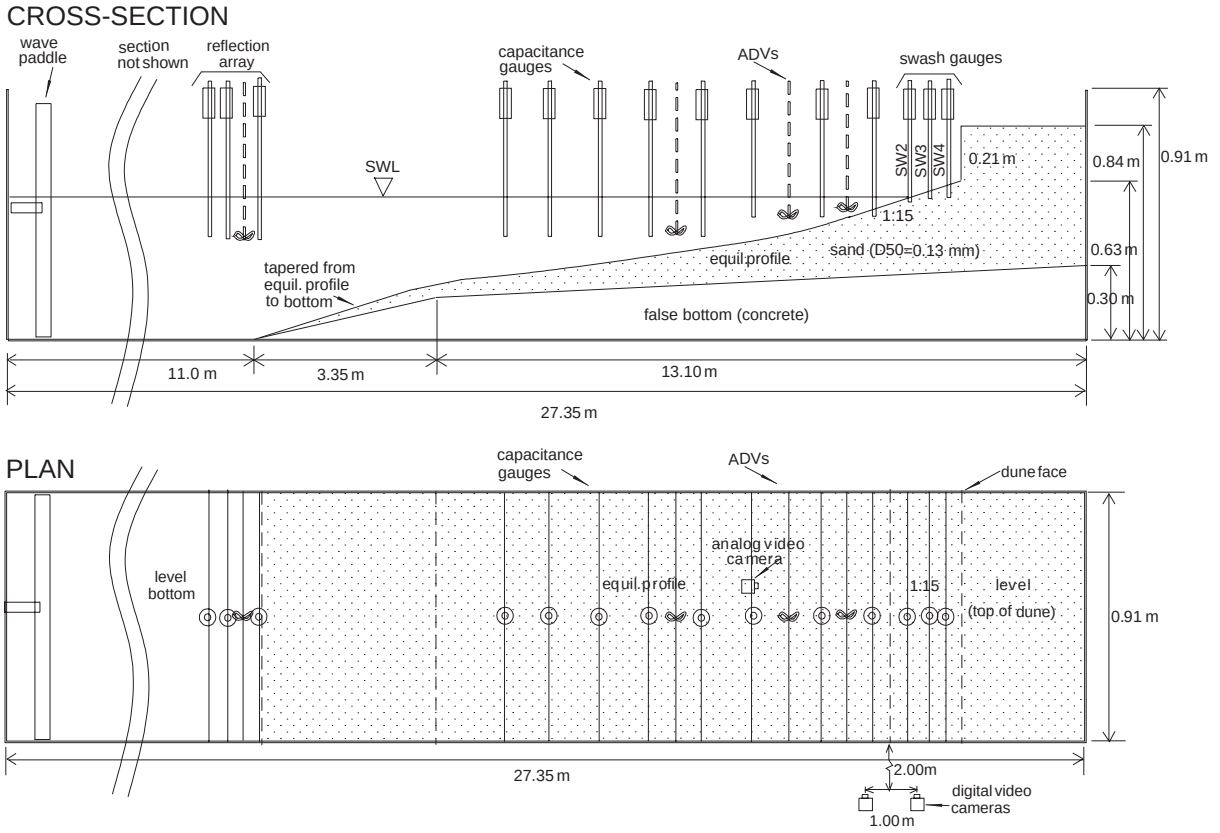

Fig. 4. Laboratory experiment arrangement. A cross section of tank is shown in upper plot and a plan view is shown in lower plot.

0.13 mm. The beach profile beneath the still-water level (SWL) was graded to represent an equilibrium profile (Dean, 1977). The beach slope from just below the SWL to the dune was 1:15. An idealized shape, in the form of a vertical face (with a height of $D = 0.21$ m), was formed to represent a dune undergoing erosion (e.g., Edelman, 1968).

Solitary waves, generated by a piston-type paddle, propagated along the length of the tank and were measured with capacitance wave gages and video cameras in the surf and swash zones. Results for the three swash gages (SW2, SW3, and SW4) partially buried in the sand and located above the SWL in the swash zone as shown in Fig. 4 are presented. All gages were calibrated daily and are estimated to measure with an accuracy of ± 2.5 mm.

Two digital video cameras (Sony, models PC100E and TRV6E, respectively) were used to record the waves and profile change in the surf zone, swash zone, and at the dune or beach. The cameras were of the PAL Western Europe and Australian standard with a captured image resolution of 720×576 pixels at 25 frames per second. The sampling frequency of the capacitance wave gages was set to 25 Hz to match the cameras. The cameras were mounted on standard tripods and positioned approximately 2 m from the sidewall of the tank (see Fig. 3) so that the swash zone and dune were viewed in one camera and the surf zone in a second camera. The cameras were placed low to the ground so that the field of view was angled looking up to the area of interest. This was done to avoid the three-dimensional effect of the waves when moving horizontally across the field of view (i.e., filming the width of the wave across the tank). Approximate camera locations are shown in Fig. 4. As the cameras were positioned about 2 m from the target, nominal pixel resolution was about 2 mm with a horizontal field of view (FOV) less than 1.5 m for each camera. The camera positions allowed overlapping fields of view showing a common board noting the date, case number, and wave conditions. Accurate time synchronization between the cameras and the gage logger was not possible due to logistical difficulties. A digital clock was displayed in the common camera FOV to assist in image synchronization, but the digital display did not show up well in the images. The water was dyed fluorescent green and a black backdrop was placed on the opposite side of the wave tank to improve image contrast. A grid of control points was marked on the outside of the glass tank wall (target plane) with an origin defined at the SWL to allow post-processing rectification.

Change of the movable bed was measured with a standard manual profiler with a 4-cm diameter disk at the bottom and a vertical resolution of ± 3 mm. For cases where a notch or overhang formed at the dune, the profiler was not used as it was not readily feasible to measure such forms with the profiler. Instead, a transparent sheet was placed on the outside of the glass tank wall in the region of the dune face and profiles were traced with a permanent marker following each wave impact.

The procedure developed for this study requires that camera placement remains constant while the camera is turned on. The procedure is as follows:

- place at least four permanent control points on the glass sidewall of the tank;
- position camera at some distance from the target plane (i.e., tank sidewall) depending on desired resolution;
- provide uniform lighting on the target plane and a uniformly colored background on the opposite sidewall (to block any unwanted objects from the FOV);
- place a removable target grid with evenly spaced control points on the outside of the tank glass wall (target plane) and in the camera's FOV;
- film target grid briefly and remove; and
- film the hydro- and morphodynamics of interest. If the camera is moved the target grid should be filmed again.

The four permanent control points (in step 1 of the above list) provide a means to verify that the camera is not moved during filming. If the pixel location of any of the control points changes from one frame to another in a coherent sequence of filmed frames, then camera movement has occurred and the filmed target grid (step 5) is not valid for the later frames. If it is known that the camera is moved during filming, a valid target grid can be obtained by replacing and re-filming the grid. Alternatively, the permanent control points may be sufficient for image rectification and used in place of the removable target grid, depending on the sought after accuracy and lens quality.

For this study, a total of 858 control points were spaced at 3 cm vertical and horizontal intervals on a removable target grid. Because the image resolution was approximately 2 mm per pixel, the spacing corresponds to approximately 15 pixels (2–3% of the total number of pixels in the vertical and horizontal directions). A grid with larger spacing in the center would probably have been sufficient considering that while lens distortion is usually the largest source of error, the lens elements are typically placed with high precision on the same optical axis so that distortion is almost always radially symmetric (Tsai, 1987; Ojanen, 1999). However, the relation between accuracy and the number of control points was not tested in this study.

The six-step procedure listed above was not exactly followed in this study as the removable target grid was not available at the original time of filming. Instead, the target grid was filmed at a later time with the camera

replaced to its original location based on measured camera positions and tilt. The permanent control markers on the target plane were used to verify the repositioning of the cameras to their original locations. Repositioning was difficult, but eventually successful, and supports the notion that implicit calibration methods (Section 2.2), whereby knowledge of exact camera locations are not necessary, are suitable for this type of laboratory experiment.

There are several benefits if the six-step procedure described above is followed: intrinsic camera parameters and accurate measurements of camera positions are not necessary, a suite of control points instead of a fine meshed grid are sufficient, and the camera can be moved between takes (with the condition that the target grid is filmed again). In most tank studies using imaging, a fine meshed grid is placed on either the glass wall between the wave and the camera or on the glass wall opposite the camera. This can be problematic when tracing waveforms. The grid on the camera side of the tank may block part of the image so that interpolation between known points is necessary. In addition, the grid lines, either on the tank wall near or opposite the camera, disrupt or complicate automatic image analyses performed after the experiment. Additionally, a grid on the opposite side of the tank (behind the wave) has the potential to be interpreted incorrectly as it is not in the same focal plane as the objects of interest.

4. Video image post-processing

Following filming in the laboratory, a number of tasks were done to obtain the hydrodynamic and geomorphic data from the video film: image capture, image rectification, and data extraction. These tasks are described in chronological order below.

4.1. Image capture

Image capture was carried out on a PC-based system (451 MHz) with the Windows 2000 platform and 130 MB of RAM memory. A high-speed interface card, IEEE 1394 FireWire™, was used to transfer digital data from the camcorder to the computer. The software package by Adobe, Premiere version 6.0, was used to capture video clips and export them to sequential bitmap files. Individual frames were de-interlaced by interpolating between the dropped rows as described previously. The still images were kept in the uncompressed bitmap format so that information would not be lost (e.g., Chapman and Chapman, 2000). Before extracting wave and profile data, each image was corrected with respect to lens distortion and camera position as discussed below.

4.2. Image rectification

A MATLAB routine was developed to physically rearrange the image pixels to correct for intrinsic camera parameters (mostly lens distortion) and camera placement. The basic premise of the method is that the pixels of an image showing a number of control points can be moved to their correct positions if the exact relative locations of the control points are known and with the assumption that the area between the control points is distorted linearly. A flow chart showing the basic components of the image correction routines is depicted in Fig. 5. Inputs to the model are a photographed image of the target sheet, and target dimensions (spacing between control points in the x- and y-directions). A virtual target grid based on measured dimensions, is then generated and anchored to one control point on the filmed target with known real world coordinates. Each pixel on the image of the filmed target is first checked if it is within a boundary defined by the outer control points of the virtual target grid, and then located, and referenced to the closest four target dots. Pixels are then physically moved to a new location based on the proximity of the four nearest target dots as shown in Fig. 6. In the figure, ♦ denotes the target dots/grid as determined by physically measuring the distances between dots, ● represents the location of the photographed dots, and ■ the pixel between target dots. The displacement required to move each pixel can be calculated using a finite difference nearest neighbor scheme:

$$\begin{aligned} \mathrm{d}x^i &= E_h^i + F_h^i x^i + G_h^i y^i + H_h^i x^i y^i, \\ \mathrm{d}y^i &= E_v^i + F_v^i x^i + G_v^i y^i + H_v^i x^i y^i, \end{aligned} \tag{1}$$

where $\mathrm{d}x^i$ and $\mathrm{d}y^i$are the x- and y-displacements of the ith pixel; x^i and y^i are x and y coordinates of the ith pixel; E through H are coefficients for the displacement of the ith pixel; and h and v denote the x- and y-directions (horizontal and vertical directions).

The coefficients are solved from a set of linear simultaneous equations:

$$\begin{aligned} \mathrm{d}x_A^i &= E_h^i + F_h^i x_A^i + G_h^i y_A^i + H_h^i x_A^i y_A^i, \\ \mathrm{d}x_B^i &= E_h^i + F_h^i x_B^i + G_h^i y_B^i + H_h^i x_B^i y_B^i, \\ \mathrm{d}x_C^i &= E_h^i + F_h^i x_C^i + G_h^i y_C^i + H_h^i x_C^i y_C^i, \\ \mathrm{d}x_D^i &= E_h^i + F_h^i x_D^i + G_h^i y_D^i + H_h^i x_D^i y_D^i, \end{aligned} \tag{2}$$

and in the y-direction:

$$\mathrm{d}y_A^i = E_v^i + F_v^i x_A^i + G_v^i y_A^i + H_v^i x_A^i y_A^i,$$

$$\mathrm{d}y_B^i = E_v^i + F_v^i x_B^i + G_v^i y_B^i + H_v^i x_B^i y_B^i,$$

$$\mathrm{d}y_C^i = E_v^i + F_h^i x_C^i + G_v^i y_C^i + H_v^i x_C^i y_C^i,$$

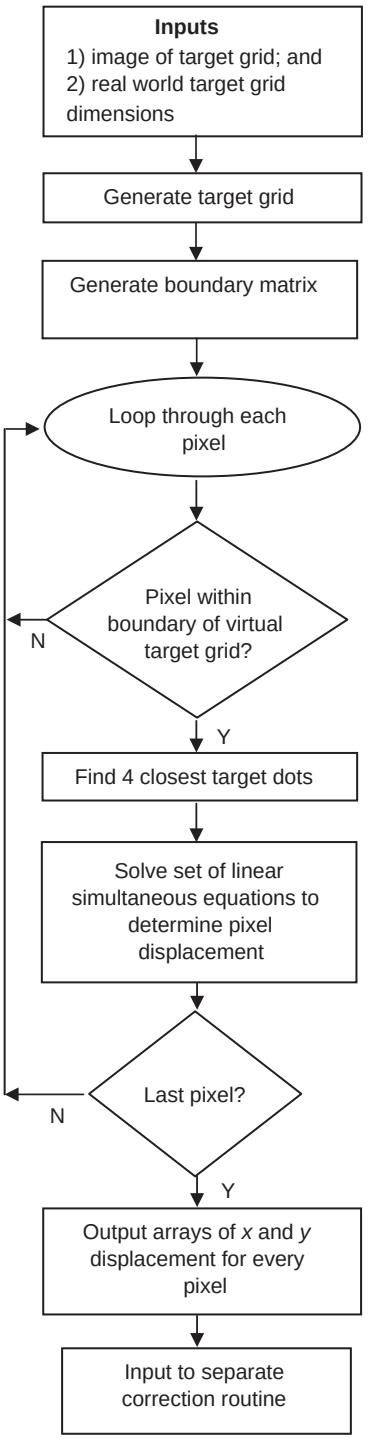

Fig. 5. Flow chart showing basic components of image correction routine.

$$dy_D^i = E_v^i + F_v^i x_D^i + G_v^i y_D^i + H_v^i x_D^i y_D^i,$$

where A, B, C, and D denote the true target locations.

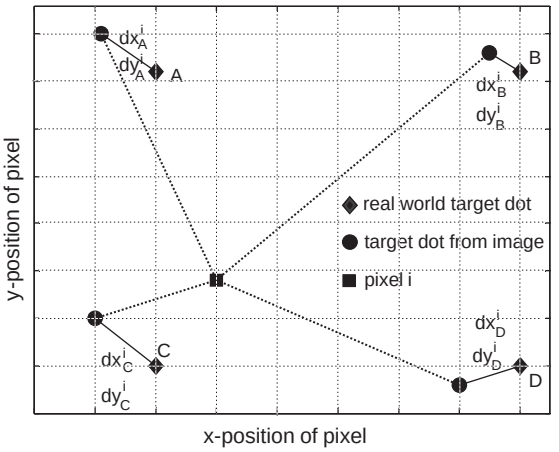

Fig. 6. Schematic showing physical relation and movement of individual pixels for image correction.

4.3. Data extraction

A semi-automatic tool for extracting wave and morphodynamic profiles from consecutive video images was developed for this study. A number of techniques, both existing and newly developed techniques, have been assessed and evaluated. A MATLAB routine partially employing a subroutine by Lau (1997) is used to extract pixels demarcating the sand bottom from water, and the water (i.e., wave) from air. The data extraction program was written so that it is also possible to employ MATLAB's edge command in the signal processing toolbox (other edge detection routines as described by Schröder et al. (2000) for example, could also be incorporated). Results using Lau's routine or the 'Roberts' edge command in MATLAB produced the best results for the images obtained in this study.

The two methods differ in that Lau's method starts at a given pixel and isolates all neighboring pixels with values within a preset tolerance. The edge command, on the other hand, looks for pixel value gradients between adjacent pixels. A problem is automating the tracing under 'roofing' conditions; when notching of the dune occurs or when the wave begins its reflection following impact with the dune. In the case of the returning bore, water mass is doubled over so that more than one y-value can be associated to a specified x-coordinate.

The traceline extraction program is set up so that numerous images can be processed automatically if filenames are consecutively numbered. An example is shown in Fig. 7 where three consecutive frames were automatically digitized with minimum user input. The tracelines are shown with solid white lines. The dash-dotted lines have been added to visually decipher the bottom and dune profiles from the water and background. The images are consecutive so that the time-lag

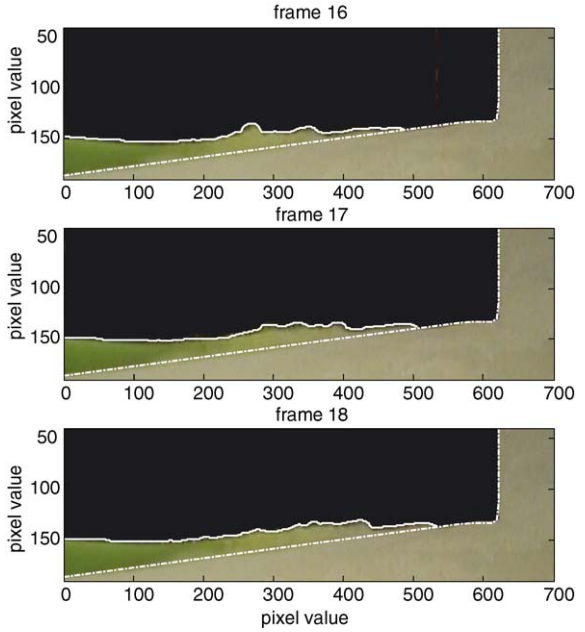

Fig. 7. Consecutive frames showing tracelines of a swash bore climbing beach at 1/25th second intervals.

between images represents the sampling frequency of the camcorder, 25 Hz.

Because the extraction (and image rectification) process is done in MATLAB, it is straightforward to continue the analysis and automatically calculate the area and change between consecutive waveforms or sand profiles extracted from the images. By maintaining all the steps of image correction, data extraction, and data analysis in the same software package, it is possible to streamline the process, increase efficiency, and process large amounts of data.

5. Results

5.1. Image rectification

Image rectification results are presented for (1) the intrinsic camera parameters, and (2) for both intrinsic and extrinsic parameters. An estimate of the error associated with the intrinsic parameters (lens distortion) was estimated by filming the target sheet so that the camera focal plane and the target points were coplanar. Fig. 8 illustrates the lens distortion recorded by the camcorder used in the study. Circles denote the real world target grid and + 's mark the photographed target dots. For this particular camera lens, the greatest error appears to be in upper and lower portions and to the right of the central axis of the image. Based on an algorithm written by Ojanen (1999), the maximum error is on the order of three pixels with a mean error of about

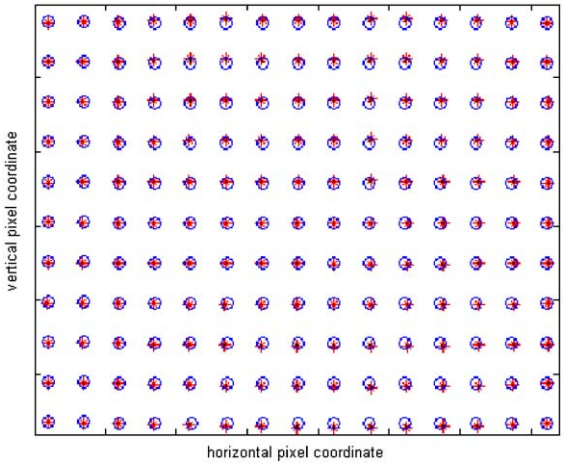

Fig. 8. Illustration of radial lens distortion recorded by 42 mm camcorder lens used in study.

1 pixel. This corresponds to an absolute real-world error of 2–6 mm at the resolution employed for this study.

Correction of both intrinsic and extrinsic camera parameters was tested using the algorithm described in the previous section. An example of a target sheet consisting of several hundred dots is shown in Fig. 9. Fig. 9A shows the original image as photographed with the camera tilted, while Fig. 9B shows the corrected image. Note that some pixel information is lost due to the camera perspective and the loss of target dots along the edges. The pixel error associated with the particular set-up and image shown in Fig. 9 is on the order of 12 pixels in the x-direction and six pixels in the y-direction. The pixel displacement is highly dependent on the camera position and can vary substantially. As seen previously, the maximum error associated with this particular camera lens is three pixels, so the remaining nine-pixel error in the x-direction and three-pixel error in the y-direction is expected to be due to camera tilt.

5.2. Comparison of data extracted from video images with data measured by conventional instruments

A comparison of data extracted from video images with data measured by conventional instruments was done to ascertain the approximate accuracy of the data extraction process described in Section 4. The comparisons are not necessarily meant to validate the procedure as there are inherent errors with conventional instruments, as well; rather, the comparisons aim to justify the use of video images as an alternative method for measuring wave and profile change data.

5.2.1. Bottom profile

A total of 18 profiles of the inner surf and outer swash zones were measured using a manual profiler and video

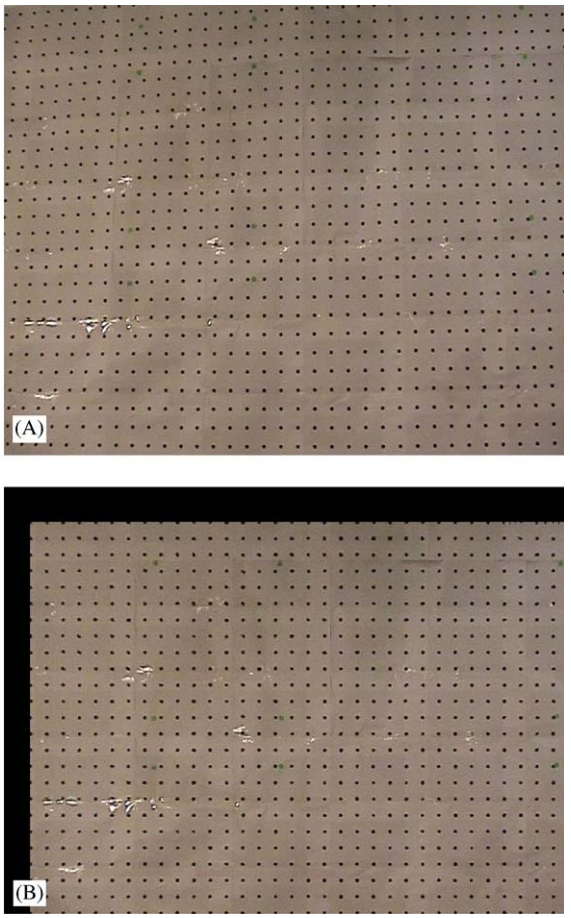

Fig. 9. Example of an uncorrected (A) and corrected (B) target sheet.

images. The manual profiler had a vertical accuracy of ± 3 mm and consisted of a standard graded rod with a 4-cm disk at the bottom. Comparison of the two measurements techniques shows good agreement with a mean difference of 5 mm.

The difference in measurement is partly due to the profiler measuring near the center of the tank while the images are determined from the profile along the glass wall of the tank. It was assumed that profile changes were uniform across the tank; this was visually observed to be true in many but not all cases where small mounds of sand were frequently noted shoreward of the gages. It should also be pointed out that any effects the sides of the tank may have had on the bottom profile are embedded in the data set using the video imaging technique. No direct visual evidence of "wall effects" was noted during the experiment, however.

5.2.2. *Dune profile*

Because the dune profile was either nearly vertical or consisted of a notch resulting from the impact of bores, it was difficult and inaccurate to use a conventional profiler to measure the shape. Instead, dune profiles were traced on a transparent sheet attached to the outside of the glass tank wall. Although tracing on transparencies is not considered a conventional measurement technique, it provides a means for comparison to data obtained with video images.

The accuracy of tracing on transparent sheets was evaluated by generating a target grid of 336 evenly spaced dots (6 mm in the x-direction and 5 mm in the y-direction). The "test" target sheet was taped on the inside of the glass tank wall to mimic the location of the side view of the dune profile. A transparent sheet was then placed on the outside of the glass wall and the dots were traced with a permanent felt marker. The dots on the "test" target sheet were traced during three separate trials. Results from one of the trials are shown in Fig. 10 in the form of a vector plot (arrows point from traced dot to target dot). The transparent sheets were scanned and the traced dots were digitized and compared to the location of the target dots. A modified form of the Mean Absolute Error (MAE) (Willmott, 1982) was used to estimate the accuracy of tracing on transparent sheets (error between a traced dot and its target location):

$$MAE = \frac{\sum \left| \sqrt{(x_{trgt} - x_{trace})^2 + (y_{trgt} - y_{trace})^2} \right|}{N}, \qquad (3)$$

where x_{trgt} and $y_{trgt} = x$ and y coordinates of a target dot, x_{trace} and $y_{trace} = x$ and y coordinates of a traced dot and $=$ number of dots.

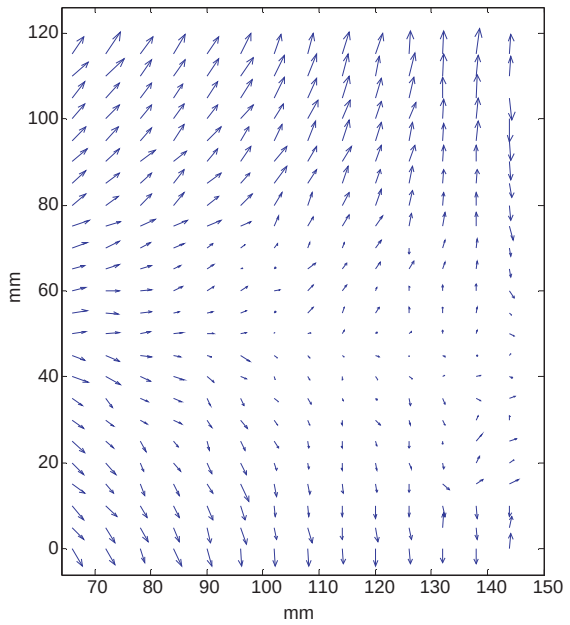

Fig. 10. Vector plot showing error between traced and target dot locations.

An average of three tracings of the "test" target indicates that the MAE is on the order of ±4 mm. The estimated accuracy is highly dependent on the ability and consistency of the person doing the tracing, and as such the estimated ±4 mm accuracy is probably only valid for this study. During the trials it was noted that there was a tendency for the tracer to move and thus change the perspective so that projections from the target plane onto the transparent sheet changed.

Fig. 11 shows results of one case where dune profiles were measured following the impact of every other bore by (1) tracing with a marker on a transparent sheet (dashed lines), and (2) digitizing corrected video images (solid lines). The digitized video images were done by hand as the automatic tracing routine is not able to handle conditions where there is more than one y-value for a given x-coordinate. Inclusion of overhangs in the automatic tracing routine would reduce human error introduced by tracing the profiles manually. Attempts to develop such a routine were made but were unsuccessful. An analysis of the nine profiles shown in Fig. 11 along with nine additional profiles from a separate experimental case indicate a mean measured difference of 3 mm of the shoreward most point of each notch using tracings or digitized images. The maximum measured difference was 5 mm.

5.2.3. Wave height

Wave heights in the swash zone were compared with measurements obtained from swash gages and video images. The swash gauges were calibrated daily with an accuracy of ±2.5 mm. The white vertical lines on the inset photos of Fig. 12 illustrate how a 'virtual gage' was assumed to be positioned at the same location as swash gage SW3 (46 cm from the dune face) employed in the experiment (see Figs. 4 and 13A for location). The curve in Fig. 12 represents the time-series of the swash height as obtained from the automatic tracing of the video images. The numbers plotted on the curve refer to the frame number or still image. This type of presentation shows that video images provide a useful tool in understanding the hydrodynamic processes. For instance, one might think that the peak of the curve is the maximum height of the swash wave prior to impacting the dune. This is not the case as is evident from the still images that show that the peak corresponds to the returning bore reflected from the dune face and that the swash height was really on the order of 4 cm, as opposed to 8.5 cm, prior to hitting the dune. This has been pointed out by others as well (e.g., Overton et al., 1994) but to the best of the authors' knowledge has not been previously presented in a graphic form as shown in Fig. 12.

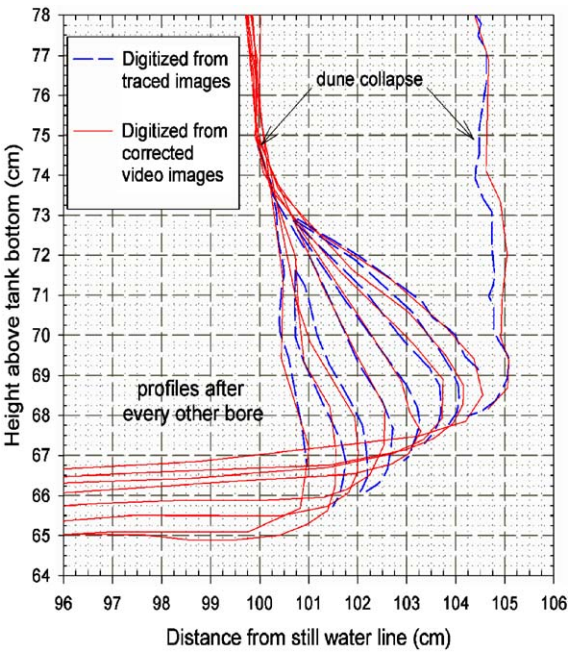

Fig. 11. Comparison of notch development at dune face from traced transparencies and corrected video images.

Comparisons of swash heights measured with capacitance gages (with sandbed offsets removed following the technique described in Kraus and Smith, 1994) and video images are shown in Fig. 13. Locations of the three swash gages are shown in Fig. 13A. The wave profile at 5.4 s after the onset of swash motion is also shown. The remaining plots show the swash heights over time as measured by the gages and video images. The camcorder and gage were not synchronized and therefore the placement along the x-axis of the two curves is somewhat subjective. However, it is clear that there is good agreement between the two measurement techniques. The overall mean difference between the two measurement techniques is 4 mm and the peak values are well represented in all cases with the largest error being 3 mm for SW2. The largest discrepancy between the measurement techniques is during the uprush between 3.7 and 5.4 s for all cases, with the greatest difference being 1.3 cm for SW3. Because the largest discrepancy lies within the same time window for all gages it is speculated that the uprush was not completely even across the tank and that it was slightly higher in the center as compared to the side of the tank.

5.2.4. Summary and comparison of data obtained from video images and conventional instruments

Table 1 summarizes and compares the mean measured difference between data obtained from digitized images and conventional instruments. Measurements are compared for bottom and dune profiles, and wave heights. The second column in Table 1 lists the accuracy of the conventional instruments used in this study. Bottom

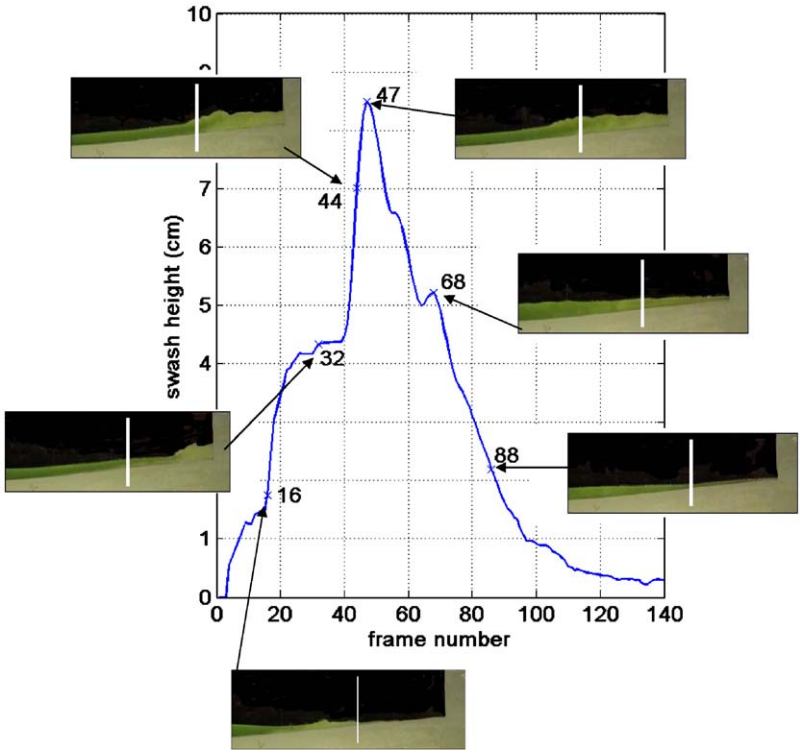

Fig. 12. Swash heights as recorded by video images at location identical to swash gauge SW3. Still images for selected frames are shown.

profiles were measured with a standard manual profiler, wave heights with conventional capacitance wave gauges, and due to a lack of an acceptable conventional tool to measure dune profiles with overhangs, dune profiles were measured by tracing on transparent sheets attached to the outside of the glass tank wall. The third column of Table 1 lists the maximum theoretical accuracy that can be expected when comparing conventional instrument measurements with video images and is simply the positive or negative sum of conventional instrument accuracy and error due to image resolution. With the experimental setup employed for this study, the resolution of the video images was slightly better than 2 mm in the horizontal and vertical directions. The fourth and fifth columns in Table 1 list the mean and maximum differences of measurements obtained with conventional instruments and video images, respectively. For all three measured subjects, the mean measured differences are less than or equal to the maximum theoretical accuracy. The maximum measured differences should also fall within the range of the theoretical accuracies; however, this is not the case for the bottom profile and wave heights. Possible explanations for this discrepancy are discussed in the following section.

6. Conclusions and discussion

Comparisons of morpho- and hydrodynamic measurements using conventional instruments and video cameras show good agreement. The mean discrepancies between the measurement techniques are within or near the normal accuracy of the measurement systems indicating that video images are valid tools for quantifying hydrodynamic and geomorphological changes in the swash zone of wave tank studies.

Differences between measured values using conventional instruments and video images of bottom and dune profiles and wave heights were summarized in Table 1. The mean of the differences between the two measurement techniques are 5, 3, and 4 mm for the bottom profiles, dune profiles, and wave heights, respectively. Maximum wave heights (up to 10 cm) were well represented with the largest error being 3 mm. The mean measured differences are all within the range of the maximum theoretical accuracy (column 3, Table 1). However, the maximum differences between the measurement techniques are outside the range of the theoretical accuracy. There are a number of possible explanations for this. The image rectification procedure may have contained an insufficient number of target

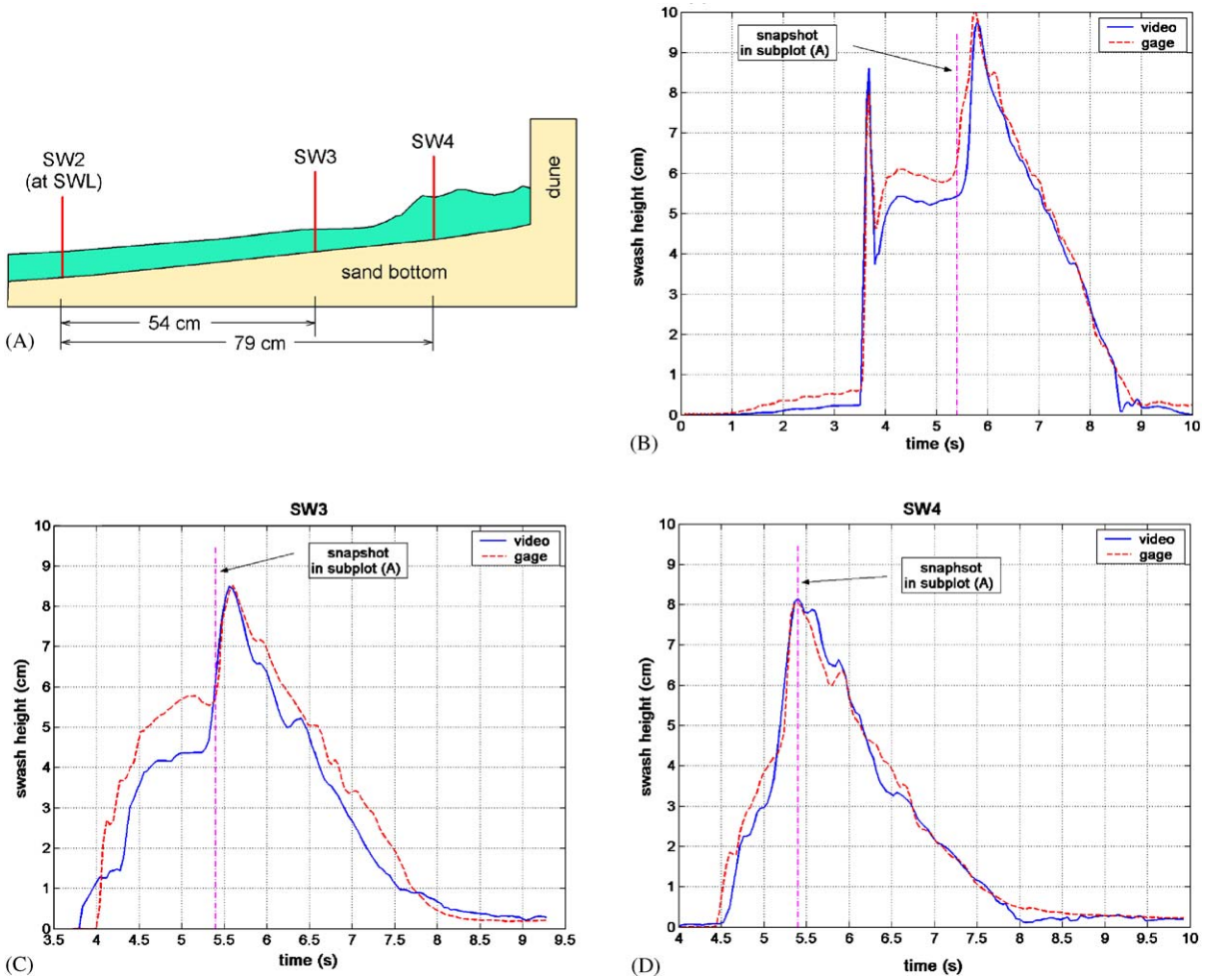

Fig. 13. Comparison between swash heights measured with capacitance gages and video images. Subplot (A) shows setup of gages and a snapshot in time for $t = 5.4$ s from onset of swash motion. Subplots B, C, and D show time series signals of swash heights for gages SW2, SW3, and SW4, respectively.

Table 1
Comparison of theoretical accuracies to variation of geomorphological and hydrodynamic measurements using conventional instruments and video images

Measured subject	Conventional instrument accuracy (mm)	Maximum theoretical accuracy[a] (mm)	Mean measured difference (mm)	Maximum measured difference (mm)
Sand bottom	±3	5	5	9
Dune face	±4	6	3	5
Wave	±2.5	4.5	4	13

[a]Conventional instrument error + error due to image resolution.

dots or introduced errors by not matching the target dots on the target sheet exactly. An analysis of the presented method's sensitivity to the number of target dots could be done, but was not for this study as there may be other reasons for the discrepancy and the obtained accuracy was deemed sufficient to justify the use of video imagery as a tool for data collection in wave tank studies. Another reason for the discrepancy may be due to entrained sand particles, picked up by the turbulent bore at and after impact with the dune, which

caused the color of the water to change affecting the ability of the tracing program to automatically decipher the transition between air and water. In addition, foam on the glass of the tank's sidewall caused the automatic tracing routine to sometimes incorrectly recognize a wave shape. As a result, digitization by hand was sometimes necessary and may have caused some inconsistencies in the objective evaluation of the wave shape.

Differences between the measured values using the two different measuring systems may in fact represent true values as considered by Foote and Horne (1999a). The experiment was designed with the intention that the waves and profile were even across the tank. However, the bottom profile was observed to be uneven at times, particularly shoreward of the gages where a build up of sediment was noted. And although visual observations suggest that the swash waves were even across the tank, there may have been some differences during the uprush of the signals that were too fast to be noted with the naked eye. The fact that time series signals of the swash heights agree very well within the resolution of the measurement techniques during the whole event except during the uprush, suggests that there was a true difference between the wave heights at the center of the tank as compared to the side. The slight variation of the wave height across the tank was probably due to the buildup of sediments shoreward of the gages or possibly the presence of the glass wall providing some friction. Irrespective of the cause for the variation, using video imagery for the collection of wave tank data to describe hydrodynamics and its effect on bottom and dune profiles should be valid given that all the measurements are obtained along the same plane along the tank wall.

Acknowledgments

The laboratory data-collection effort was supported by the Coastal Inlets Research Program, US Army Corps of Engineers. Additional financial support was provided by VINNOVA (Swedish Agency for Innovation Systems) under the project titled "The interaction of large and high speed vessels with the environment in archipelagos." The authors thank Dr. Nicholas C. Kraus at the US Army Engineer Research and Development Center, Coastal and Hydraulics Laboratory, Professor Magnus Larson at Lund Institute of Technology, Dr. Atilla Bayram at Han Padron, Associates, and Dr. Rolf Erikson at BBL for valuable support, discussions, and ideas.

References

Aagaard, T., Holm, J., 1989. Digitization of wave run-up using video records. Journal of Coastal Research 5 (3), 547–551.

Chapman, N., Chapman, J., 2000. Digital Multimedia. Chichester, Wiley, UK 568pp.

Dean, R.G., 1977. Equilibrium beach profiles: US Atlantic and Gulf Coasts. Ocean Engineering Report 12, Department of Civil Engineering, University of Delaware, Newark, 45pp.

Edelman, T., 1968. Dune erosion and storm conditions. In: Proceedings of the Fourth International Conference on Coastal Engineering, London, England, pp. 719–722.

Fenaish, T.A., Overton, M.F., Fisher, J.S., 1989. Dune erosion and sediment profile due to wave uprush. In: Proceedings of the 21st International Conference on Coastal Engineering, Sol-Malaga, Spain, pp.1426–1436.

Foote, M., Horn, D., 1999a. Video measurement of swash zone hydrodynamics. Geomorphology 29, 59–76.

Foote, M., Horn, D., 1999b. Swash zone velocity and volumetric measurement using a simple video technique. In: Proceedings of the Fourth International Symposium on Coastal Engineering and the Science of Coastal Sediment Processes, Long Island, NY, pp. 393–404.

Holland, K.T., Holman, R.A., 1997. Video estimation of foreshore topography using trinocular stereo. Journal of Coastal Research 13 (1), 81–87.

Holland, K.T., Holman, R.A., Sallenger, A.H., 1991. Estimation of overwash bore velocities using video techniques. In: Proceedings of the Third International Symposium on Coastal Engineering and the Science of Coastal Sediment Processes, Seattle, WA, pp. 489–496.

Holland, K.T., Puleo, J.A., Kooney, T.N., 2001. Quantification of swash flows using video-based particle image velocimetry. Coastal Engineering 44, 65–77.

Hughes, M.G., 1992. Application of a non-linear shallow water theory to swash following bore collapse on a sandy beach. Journal of Coastal Research 8 (3), 562–578.

Kraus, N.C., Smith, M.J., 1994. SUPERTANK laboratory data collection project, vol. I: Main text. Technical Report CERC-94-3, US Army Engineer Waterways Experiment Station, Vicksburg, MS., 274pp.

Lau, D.L., 1997. Magicwand. ftp://ftp.mathworks.com/pub/contrib/v5/image/magicwand.c

Larson, M., Sunamura, T., 1993. Laboratory experiments on flow characteristics at a beach step. Journal of Sedimentary Petrology 63 (3), 495–500.

Lippman, T.C., Holman, R.A., 1989. Quantification of sand bar morphology: a video technique based on wave dissipation. Journal of Geophysical Research 94 (C1), 995–1011.

Lippman, T.C., Holman, R.A., 1990. The spatial and temporal variability of sand bar morphology. Journal of Geophysical Research 95 (C7), 11575–11590.

Lippman, T.C., Holman, R.A., 1991. Phase speed and angle of breaking waves measured with video techniques. In: Proceedings of the Third International Symposium on Coastal Engineering and the Science of Coastal Sediment Processes, Seattle, WA, pp. 542–556.

Ojanen, H., 1999. Automatic correction of lens distortion by using digital image processing, http://www.iki.fi

Overton, M.F., Fisher, J.S., 1988. Laboratory investigation of dune erosion. Journal of Waterway, Port, Coastal, and Ocean Engineering 114 (3), 367–373.

Overton, M.F., Fisher, J.S., Fenaish, T., 1986. Numerical analysis of swash forces on dunes. In: Proceedings of the

Fourth International Conference on Coastal Engineering, Taipei, Taiwan, pp. 632–641.

Overton, M.F., Fisher, J.S., Hwang, K.-N., 1994. Development of a dune erosion model using Supertank data. In: Proceedings of the 24th International Conference on Coastal Engineering, Kobe, Japan, pp.2488-2502.

Redondo, J.M., Rodriguez, A., Bahia, E., Falques, A., Garcia, V., Sanches-Arcilla, A., Stive, M.J.F., 1994. Image analysis of surf zone hydrodynamics. In: Coastal Dynamics Proceedings of the First International Conference on the Role of the Large Scale Experiments in Coastal Research, Barcelona, Spain, pp. 350–365.

Ruessink, B.G., Kleinhans, M.G., van den Beukel, P.G.L., 1998. Observations of swash under highly dissipative conditions. Journal of Geophysical Research 103 (C2), 3111–3118.

Ruessink, B.G., Bell, P.S., van Enckevort, I.M.J., Aarninkhof, S.G.J., 2002. Nearshore bar crest location quantified from time-averaged X-bank radar images. Coastal Engineering 45 (1), 19–32.

Sallenger, A.H., Holman, R.A., 1987. Infragravity waves over a natural barred profile. Journal of Geophysical Research 92, 9531–9540.

Schröder, M., Walessa, M., Rehrauer, H., Seidel, K., Datcu, M., 2000. Gibbs random field models: a toolbox for spatial information extraction. Computers & Geosciences 26 (4), 423–432.

Smith, E., Kraus, N.C., 1990. Laboratory study on macrofeatures of wave breaking over bars and artificial reefs. Technical report CERC-90-12, Coastal Engineering Research Center, Waterways Experiment Station, Vicksburg, MS, 155pp.

Tsai, R.Y., 1987. A versatile camera calibration technique for high-accuracy 3D machine vision metrology using off-the-shelf TV cameras and lenses. Journal of Robotics and Automation RA(3), 323–344.

Willmott, C.J., 1982. Some comments on the evaluation of model performance. Bulletin of the American Meteorological Society 63 (11), 1309–1313.

Wright, P., 1976. A cine-camera technique for process measurement on a ridge and runnel beach. Sedimentology 23, 705–712.